A mechanistic model to predict effects of cathepsin B and cystatin C on β-amyloid aggregation and degradation

Tyler J. Perlenfein and Regina M. Murphy[1]

From the Department of Chemical and Biological Engineering, University of Wisconsin, Madison, Wisconsin 53706

Edited by Paul E. Fraser

β-Amyloid (Aβ) aggregation is thought to initiate a cascade of neurodegenerative events in Alzheimer's disease (AD). Much effort is underway to develop strategies to reduce Aβ concentration or inhibit aggregation. Cathepsin B (CatB) proteolytically degrades Aβ into non-aggregating fragments but is potently inhibited by cystatin C (CysC). It has been suggested that decreasing CysC would facilitate Aβ clearance by relieving CatB inhibition. However, CysC binds Aβ and inhibits Aβ aggregation, suggesting that an intervention that increases CysC would prevent Aβ aggregation. Both approaches have been tested in animal models, yielding contradictory results, possibly because of the opposing influences of CysC on Aβ degradation *versus* aggregation. Here, we sought to develop a model that quantitatively predicts the effects of CysC and CatB on Aβ aggregation. Aβ aggregation kinetics in the absence of CatB or CysC was measured. The rate constant for Aβ degradation by CatB and the equilibrium constant for binding of CysC to Aβ were determined. We derived a mathematical model that combines material balances and kinetic rate equations. The model accurately predicted Aβ aggregation kinetics at various CatB and CysC concentrations. We derived approximate expressions for the half-times of degradation and aggregation and show that their ratio can be used to estimate, at any given Aβ, CatB, or CysC concentration, whether Aβ aggregation or degradation will result. Our results may be useful for designing experiments and interpreting results from investigations of manipulation of CysC concentration as an AD therapy.

Alzheimer's disease (AD)[2] is the most common cause of dementia, estimated to affect over 44 million people worldwide. According to the amyloid cascade hypothesis, the initiating event in AD occurs when the membrane-bound amyloid precursor protein (APP) is sequentially cleaved into a small peptide fragment, β-amyloid (Aβ), and secreted into extracellular fluid (1, 2). Processing of APP by a β-site-cleaving enzyme (β-secretase) initiates the amyloid secretory pathway, followed by liberation of the peptide from its transmembrane domain by a γ-site-cleaving enzyme (γ-secretase). Specificity of the γ-secretase is broad, and cleavage generates various lengths of Aβ, of which the most common are Aβ_{40} and Aβ_{42} (3). After liberation (and possibly before secretion), Aβ self-associates into small, soluble oligomers that mature into larger fibrillar structures. Eventually, aggregates precipitate and deposit on neuronal tissue as amyloid plaque. Aggregates are thought to be neurotoxic (4), with smaller Aβ oligomeric intermediates believed to be more toxic than mature fibrils (5). For this reason, the kinetics of amyloid protein aggregation have been studied extensively (6–10). Although Aβ_{40} concentration is higher than Aβ_{42} in human AD brain tissue, Aβ_{42} is believed to be more aggregation-prone and more toxic (2).

Cystatin C (CysC) is a small (13.4 kDa) extracellular protein that is ubiquitously synthesized and is at relatively high concentrations in cerebrospinal fluid (CSF) (11). The link between CysC, Aβ, and AD was identified years ago with the discovery that CysC and Aβ co-deposit in cerebrovascular and senile plaques of AD patients (12, 13) and in amyloid deposits in the cerebrovasculature of patients with cerebral amyloid angiopathy (14–16). More recently, soluble CysC–Aβ complexes were detected in CSF from AD patients (17). CysC has been reported to bind Aβ and prevent further aggregation *in vitro* (18–20) and to protect cultured neurons from Aβ toxicity (21). Binding epitopes have been proposed based on molecular docking simulations and limited proteolysis experiments (22). CSF CysC levels were reported to be lower in AD than in healthy controls (23, 24), whereas plasma CysC levels were reportedly higher in AD (25), possibly because high levels are associated with an anti-inflammatory response. CysC levels may be low in patients with mild cognitive impairment but later increase as a general response to cell damage (25).

CysC is an inhibitor of cysteine proteases, including those in the cathepsin family. Cathepsin B (CatB), a cysteine-type protease of the lysosomal/endosomal pathways, is specifically inhibited by CysC with sub-nanomolar affinity (20, 26, 27). Although CatB is mainly active intracellularly, it can be secreted. Should CatB escape the cell (in the case of apoptosis or secretory pathway activation), CysC has the important role of suppressing proteolysis in the extracellular space (28). CatB has been shown to degrade Aβ, primarily through C-terminal truncation (29). Acidic pH favors rapid sequential conversion of Aβ_{42} into Aβ_{40} and then finally to the less-amyloidogenic Aβ_{38} (30). Reaction rates are slower at neutral pH but not completely diminished (30). CatB secretion from neuronal cells following

stimulation by Aβ aggregates has been documented (31, 32), and secreted CatB is known to retain a significant fraction of its activity (33, 34). There is conflicting data with regard to the relationship of CatB to AD; CatB was expressed at lower levels in AD patient monocytes compared with healthy controls in one study (35), but in another study, CatB levels were higher in plasma of AD patients compared with controls (36).

Because of their roles in preventing fibrillation and in degrading Aβ, manipulation of CysC or CatB has been identified as a potential AD therapeutic. However, there is disagreement as to whether CysC or CatB levels should be modulated and whether the levels should be suppressed or enhanced. Some researchers have reported neuroprotective effects of CysC enhancement in animal models. Mi *et al.* (37) found that transgenic mice expressing human CysC at ~2-fold higher levels than endogenous cystatins showed a marked decrease in Aβ fibril deposition. Kaeser *et al.* (38) showed that CysC overexpression reduced plaque formation in human APP-transgenic mice. In another study using CatB-deficient mice, overexpression of CysC reduced the total amyloid plaque load (39).

Other researchers have found evidence that CatB proteolysis of Aβ is an important neuroprotective mechanism and that high amounts of CysC interfere with Aβ degradation. CatB enhancement in transgenic AD mouse models reduced both the total amount of soluble $A\beta_{42}$ and the ratio of $A\beta_{42}/A\beta_x$, indicating CatB may preferentially degrade $A\beta_{42}$ relative to other forms (30). Sun *et al.* (39) found mice overexpressing CatB lacked symptoms of cognitive impairment and premature mortality compared with CatB-free controls. These researchers also showed that expression of CysC could neutralize the neuroprotective effects of CatB. Similarly, Wang *et al.* (40) overexpressed neuronal CatB in transgenic mice and observed significantly lowered $A\beta_{42}$ levels, without affecting APP processing. Transduction of neurons to express CatB accelerated Aβ degradation and suppressed its production *in vitro* and led to a reduction of both $A\beta_{40}$ and $A\beta_{42}$ (41). Deletion of stefin B (a cysteine protease inhibitor) in an AD mouse model reduced Aβ accumulation and inhibited development of learning and memory deficits (42).

Others interpret the outcome of studies in light of putative β-secretase activity by CatB (3, 29). Inhibition of CatB reduced plaque load and improved cognitive defects in transgenic mouse models; this was postulated to be due to reduced cleavage of APP into Aβ (43, 44). Wang *et al.* (45) found that exogenously-applied CysC reduced soluble Aβ levels in animal studies, which was attributed to CysC-mediated reduction in β-secretase activity.

Differing results in transgenic animal models may be caused by differences in concentrations of Aβ, CysC, and/or CatB. In particular, CysC plays two conflicting roles in the regulation of Aβ as follows: by binding to Aβ it can inhibit Aβ aggregation, but by binding to CatB it inhibits Aβ degradation. CysC and CatB interactions have been postulated to form key control mechanisms to regulate Aβ aggregation potential (39, 43, 47). The aim of this study was to quantify the effects of CysC and CatB on the fate of Aβ. We modeled the protein interactions by considering binding, degradation, and aggregation reactions, and then we measured each relevant thermodynamic and
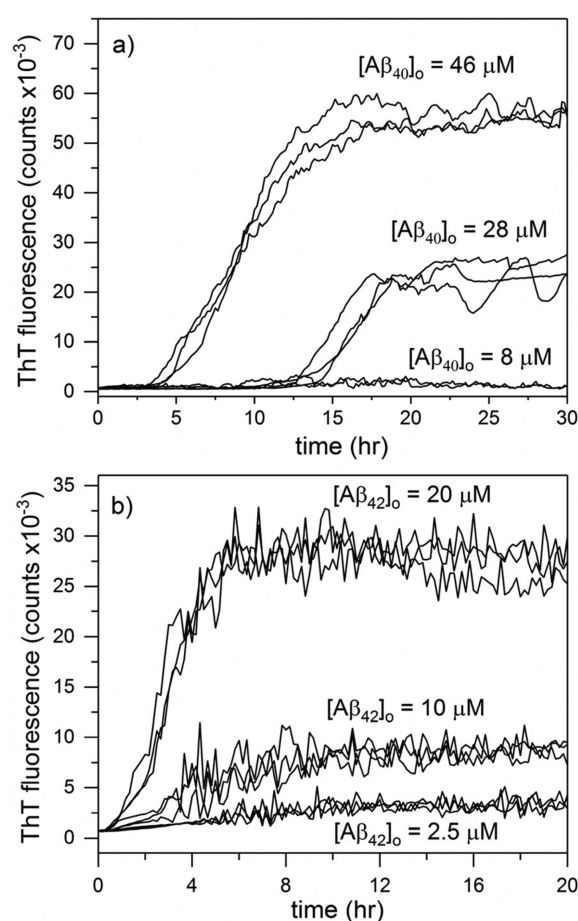

Figure 1. ThT fluorescence data of $A\beta_{40}$ (*a*) or $A\beta_{42}$ (*b*) aggregation. Three independent samples of each initial Aβ concentration were prepared, and fluorescence was measured every 10 min for up to 30 h at 37 °C.

kinetic parameter. We sought to understand the sensitivity of Aβ aggregation to perturbations in CysC/CatB balance and to be able to predict the outcome simply by knowledge of total CysC and CatB concentrations.

Results

Aβ aggregation kinetics

We measured Aβ aggregation kinetics at three different concentrations using ThT, a dye that fluoresces when bound to amyloid fibrils. Briefly, $A\beta_{40}$ (8, 28, and 46 μM) or $A\beta_{42}$ (2.5, 10, and 20 μM) was loaded into microwells and heated to 37 °C. Sample fluorescence was continuously monitored for up to 72 h. Data for each of three replicates are shown in Fig. 1. Post-aggregation, $A\beta_{40}$ at 28 μM was centrifuged, and the peptide content of the supernatant was measured. No peptide was detected (assay sensitivity <500 nM), so we concluded that all Aβs had converted to aggregated species. Therefore, at long time the fibrillar Aβ concentration (in equivalent monomer molar units) equaled the total Aβ concentration $[A\beta]_0$. To convert ThT fluorescence intensity to concentration of fibrillar Aβ, we plotted the maximum ThT signal (at 72 h) against $[A\beta]_0$ and fit the data to the polynomial shown in Equation 1,

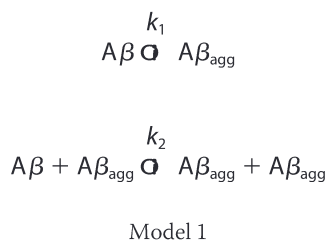$$ThT - ThT_b = a[A\beta]_0 + b[A\beta]_0^2 \qquad \text{(Eq. 1)}$$

Table 1

Parameters for conversion of ThT fluorescence intensity to [Aβ$_{agg}$] (μM)

	a^a	b
Aβ$_{40}$	33 ± 8	25 ± 10
Aβ$_{42}$	430 ± 35	44 ± 15

^{a} Parameters a and b were determined by non-linear least-squares fitting of ThT fluorescence data at 72 h to ThT − ThT$_b$ = a[Aβ]$_0$ + b[Aβ]$_0^2$ (Equation 1), where [Aβ]$_0$ is the total Aβ concentration in μM and [Aβ$_{agg}$] = [Aβ]$_0$ at 72 h. ThT$_b$ was determined by averaging three sample wells containing ThT but no Aβ and was found to be 520 ± 40. Error estimates are 95% confidence intervals.

Table 2

Kinetic and thermodynamic parameters

Error estimates are 95% confidence intervals.

	k_1	k_2	$K_D{}^a$	k_{deg}	$K_I{}^b$
	$10^{-9}\,s^{-1}$	$10^{-9}\,nM^{-1}\,s^{-1}$	nM	$10^{-9}\,nM^{-1}\,s^{-1}$	nM
Aβ$_{40}$	1.2 ± 0.4	11 ± 2	72 ± 6	1600 ± 300	
Aβ$_{42}$	5600 ± 500	17 ± 4	72 ± 6	1200 ± 300	
CatB					0.3

^{a} K_D for CysC-Aβ$_{42}$ was assumed to be identical to that measured for CysC-Aβ$_{40}$.
^{b} Values were obtained from Refs. 20, 26, and 27.

where ThT$_b$ is background signal, and a and b were determined by least-squares fitting (Table 1).

Equation 1 was used to convert ThT intensity at all time points to [Aβ$_{agg}$], where [Aβ$_{agg}$] is the concentration of aggregated Aβ expressed in equivalent monomer molar concentration. Aggregation data were fit to several different simple kinetic models, including the monomer partitioning, Gompertz, and autocatalytic models (supplemental Fig. S1) (6, 48). The best global fits were obtained by the autocatalytic model, a two-step model that includes a first-order irreversible conversion of monomer to aggregation-competent form and a second-order reaction between monomer and aggregate to produce more aggregate (6) as shown in Model 1.

$$\text{A}\beta \;\underset{}{\overset{k_1}{\rightleftharpoons}}\; \text{A}\beta_{agg}$$

$$\text{A}\beta + \text{A}\beta_{agg} \;\underset{}{\overset{k_2}{\rightleftharpoons}}\; \text{A}\beta_{agg} + \text{A}\beta_{agg}$$

Model 1

This kinetic model has an analytical solution shown in Equation 2,

$$\frac{[\text{A}\beta_{agg}]}{[\text{A}\beta]_0} = 1 - \frac{(k_1 + k_2[\text{A}\beta]_0)\exp(-(k_1 + k_2[\text{A}\beta]_0)t)}{k_2[\text{A}\beta]_0\exp(-(k_1 + k_2[\text{A}\beta]_0)t) + k_1}$$

(Eq. 2)

where [Aβ$_{agg}$] is the monomer-equivalent concentration of Aβ aggregates at any time t. Although such a two-step model cannot account for oligomer or protofibril formation, protofibril association, fragmentation, or other events (9), it does capture the sigmoidal shape and concentration dependence of the data, and it can describe accumulation of ThT-positive aggregates. Aggregation data for six (Aβ$_{40}$) or nine (Aβ$_{42}$) independently prepared samples were globally fit to Equation 2 by least-squares regression to recover k_1 and k_2 for both Aβ$_{40}$ and Aβ$_{42}$ (Table 2). Best fit lines were generated and compared with each aggregation data set (Fig. 2). Although k_2 was similar for the two Aβ forms, k_1 was 5000-fold higher for Aβ$_{42}$ than for Aβ$_{40}$, consistent with its higher aggregation propensity.

CysC–Aβ-binding interaction

CysC co-localizes with Aβ in AD plaques (12, 49). A few studies show that CysC inhibits Aβ fibril formation *in vitro*, possibly redirecting Aβ self-association toward amorphous non-fibrillar aggregates (12, 50). It is unknown whether CysC
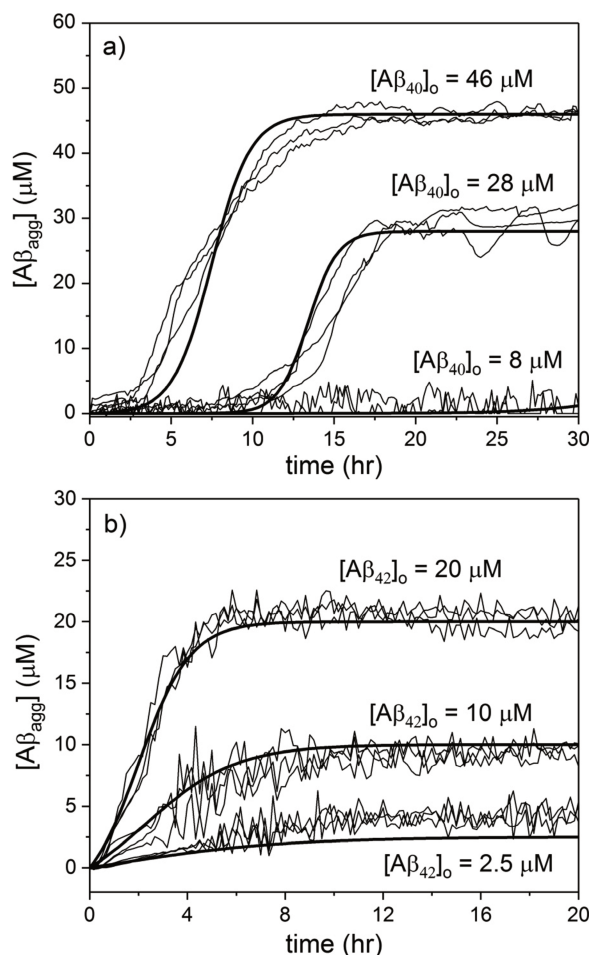

Figure 2. ThT signal was converted to [Aβ$_{agg}$] by an empirically-determined quadratic function. Autocatalytic aggregation model parameters k_1 and k_2 were derived from global fits to 28 and 46 μM (Aβ$_{40}$) (*a*) and 2.5, 10, and 20 μM (Aβ$_{42}$) data sets (*b*). Best fit lines (*bold lines*) were compared with data (*thin lines*). 8 μM (Aβ$_{40}$)$_0$ data are shown compared with model prediction. These data were not included in the data sets for parameter estimation. Because essentially no aggregation was detected, the information content is less, and the data put an upper but not lower bound on k_1 and k_2.

predominantly binds monomeric or aggregated Aβ. We designed a FRET assay to measure CysC–Aβ binding in solution (Fig. 3*a*). Data were normalized to the maximum observed FRET efficiency and expressed as a fraction of bound Aβ (Fig. 3*b*). Data from three independent series were fit globally to determine the binding constant, K_D, and the cooperativity parameter *n*. *n* was found to be 0.94 ± 0.05, so the data were re-fit with *n* = 1, to obtain a final value for K_D of 72 ± 6 nM (Table 2). Our estimate is slightly weaker than that derived from an ELISA method, where K_D was estimated to be 10 nM (50).
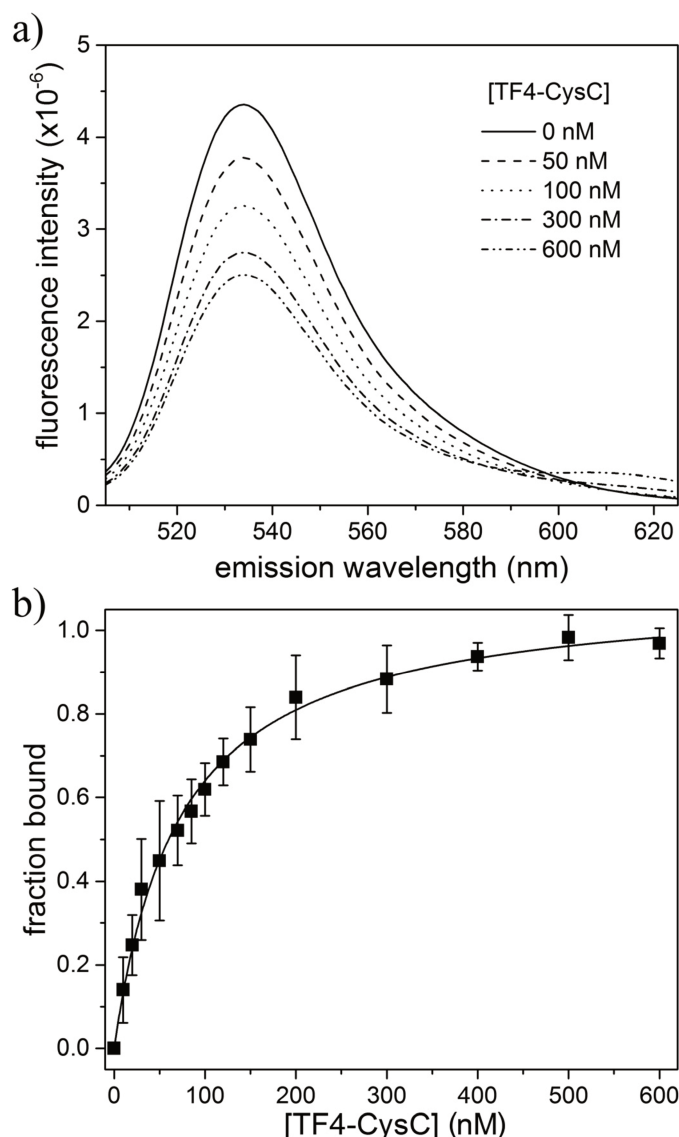
a)

b)

Figure 3. HF488-Aβ/TF4-CysC binding interaction by FRET analysis. *a,* mixture fluorescence was measured as a function of TF4-CysC, holding HF488-Aβ constant at 400 nM (excitation 488 nm). Average of three independent scans is shown for a representative set of mixtures. *b,* donor emission at 530 nm was used to calculate FRET efficiency and determine fraction of HF488-Aβ bound for each TF4-CysC concentration. Data points are the average of three independent trials. *Error bars* represent the sample standard deviation. *Solid line* is the Hill equation fit to the data, with $n = 1$.

CatB degradation of Aβ

At neutral pH, CatB proteolysis of Aβ proceeds via C-terminal truncation; products of $A\beta_{42}$ degradation were reported to be $A\beta_{40}$, $A\beta_{38}$, and $A\beta_{33}$ (30). Preliminary experiments in our laboratory were consistent with this finding (data not shown). To determine degradation rate constants, fixed concentrations of CatB were incubated with various amounts of $A\beta_{40}$ or $A\beta_{42}$ in physiological conditions (pH 7.4, 37 °C). Degradation over time was measured by dot-blot assay, where membranes were probed using antibodies specifically against the C terminus of $A\beta_{40}$ or $A\beta_{42}$ (Figs. 4*a* and 6, *a* and *b*). Measurement linearity was determined by the concentration standard curves (Fig. 4*b*), and only those samples in the linear concentration region were reported. Sample intensity was converted to Aβ concentration
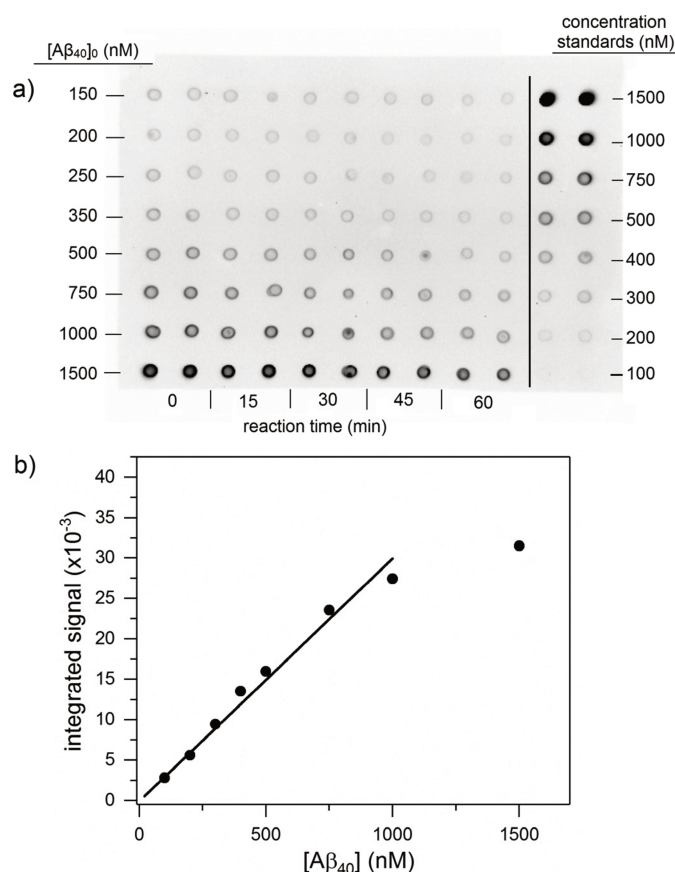
a)

b)

Figure 4. $A\beta_{40}$ degradation by CatB. *a,* sample immunoblot showing $A\beta_{40}$ degradation by CatB. Mixtures of 200 nM CatB and the listed $[A\beta_{40}]_0$ were incubated at 37 °C and pH 7.4. Samples were dotted onto the membrane in duplicate at each time point shown. Concentration standards were also dotted in duplicate. *b,* concentration standard curves were used to convert integrated signal to Aβ concentration. Signals near saturation were discarded from analysis due to non-linearity. Data points are the average of *two dots* in the concentration standards shown in *a.*

using the standard curves. $A\beta_{40}$ concentration could reliably be determined as low as 50 nM, whereas $A\beta_{42}$ could only be determined down to 200 nM. With $A\beta_{40}$, concentration decreased over time as expected (Fig. 4*a*). Concentrations over short time periods (1 h) were plotted to determine the initial reaction rate (Fig. 5*a*), and initial rates were plotted against initial Aβ concentrations to determine the degradation rate constant k_{deg} (Fig. 5*b* and Table 2). $A\beta_{42}$ degradation kinetics were measured in a similar manner (Fig. 6*a*), except $A\beta_{42}$ blots were stripped and re-probed with anti-$A\beta_{40}$ to show the generation of $A\beta_{40}$ directly from $A\beta_{42}$ as a result of CatB activity (Fig. 6*b*). Quantitative densitometry analyses at 600 nM $A\beta_{42}$ are shown (Fig. 6, *c* and *d*), demonstrating the close temporal correspondence between loss of antibody binding to the C terminus of $A\beta_{42}$ and gain of anti-$A\beta_{40}$-specific antibody binding. Values of k_{deg} for $A\beta_{40}$ and $A\beta_{42}$ were not statistically different.

CatB degradation of CysC

Optimal CatB proteolytic activity occurs in acidic conditions (pH <6), which is relevant for CatB contained within endocytic and lysosomal vesicles (51). Upon secretion to neutral CSF, CatB activity is expected to decrease, but not deactivate entirely (33, 34). Others have reported that secreted cathepsin D specif-
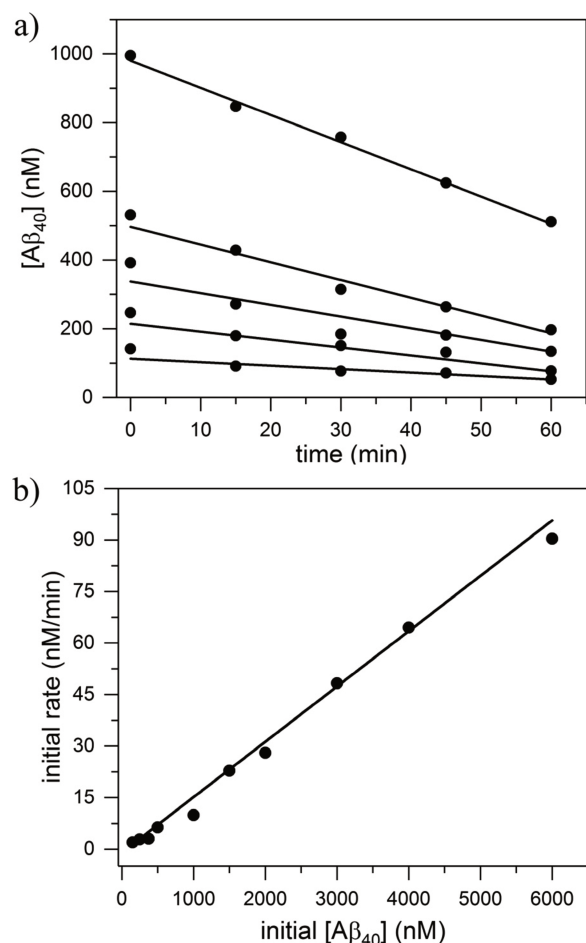
ASBMB

a)

b)

Figure 5. Aβ degradation kinetics. *a,* dot intensities of degradation samples were converted to Aβ concentrations using concentration standards and plotted as a function of time. *b,* initial rates were plotted against initial Aβ concentration. The slope of the linear fit was used to calculate k_{deg} for CatB degradation of Aβ as described under "Experimental procedures." Each point is the mean value of at least two independent measurements.

ically degrades extracellular CysC in acidic to near-neutral tumor environments (52). We speculated that CatB could similarly degrade CysC, reducing CysC inhibitory capacity and promoting uncontrolled proteolysis. When considering the interaction between CatB and CysC, a complication arises due to coupling of the inhibitory and degradation reactions. To measure true degradation kinetics, it is necessary to first "turn off" inhibitory binding modes between CysC and CatB. Using site-directed mutagenesis, we produced and purified W106G CysC, a variant which has been shown to be a poor inhibitor of CatB (53). We confirmed by CatB activity assay that W106G inhibition constant is far weaker than WT (supplemental Fig. S3). The CD spectrum of W106G was identical to WT, confirming that loss of activity is due to specific loss of interaction, rather than loss of protein fold (supplemental Fig. S2).

We used an immunoblot assay to measure the kinetics of W106G CysC degradation by CatB at 37 °C for up to 2 h. There was no detectable CysC degradation at pH 7.4 (supplemental Fig. S4). We stripped and re-probed each membrane with a CysC N-terminal antibody (C-27) and a third antibody that does not overlap with the N or C terminus (Cyst24); neither showed significant degradation (data not shown). At pH 6.0,

W106G degradation was noticeable (supplemental Fig. S4). WT was degraded much more slowly due to coupling of the inhibition reaction to degradation.

Model development

We developed a kinetic model to predict the effect of CysC and CatB on Aβ aggregation and degradation. CysC plays two distinct roles in this model: by binding to Aβ it inhibits Aβ aggregation, but by binding to CatB it inhibits Aβ degradation. We assumed all binding reactions are reversible and sufficiently fast to be assumed always at equilibrium, with equilibrium dissociation constants of K_D (binding of CysC to $A\beta_{40}$ or $A\beta_{42}$) and K_I (binding of CysC to CatB). We assumed that CysC binds only non-aggregated Aβ. Aβ is enzymatically degraded by CatB, by the rate constant k_{deg}. We assumed that CatB degrades Aβ monomers but does not degrade Aβ aggregates. Degradation of CysC by CatB was not included because it was negligible at pH 7.4.

The mathematical model includes coupled algebraic and differential equations. Material balance Equations 3 and 4 are derived assuming that the concentration of CatB bound to the substrate is negligibly small ($K_m \gg [S]$, see the supplemental text for justification). Free CatB or CysC concentration [CatB] or [CysC], respectively, at any time is calculated as the initial concentration ($[CysC]_0$ or $[CatB]_0$, respectively) minus the protein that is bound in the CysC–CatB complex or (for CysC) to Aβ, where K_D and K_I are given in Table 2.

$$[CatB] = [CatB]_0 - \frac{[CysC][CatB]}{K_I} \quad \text{(Eq. 3)}$$

$$[CysC] = [CysC]_0$$
$$- \frac{[CysC][A\beta_{40}]}{K_D} - \frac{[CysC][A\beta_{42}]}{K_D} - \frac{[CysC][CatB]}{K_I} \quad \text{(Eq. 4)}$$

Aβ monomer material balances account for decreases due to binding to CysC, enzymatic degradation, or aggregation. Additionally, $A\beta_{40}$ can be generated from $A\beta_{42}$ degradation as shown in Equations 5 and 6.

$$[A\beta_{40}] = [A\beta_{40}]_0$$
$$- \frac{[CysC][A\beta_{40}]}{K_D} - [A\beta_{40, deg}] + [A\beta_{42, deg}] - [A\beta_{40, agg}] \quad \text{(Eq. 5)}$$

$$[A\beta_{42}] = [A\beta_{42}]_0 - \frac{[CysC][A\beta_{42}]}{K_D} - [A\beta_{42, deg}] - [A\beta_{42, agg}]$$
$$\text{(Eq. 6)}$$

The rate of production of degraded or aggregated Aβ is described by differential Equations 7–10,

$$\frac{d[A\beta_{40, deg}]}{dt} = k_{deg, 40}[A\beta_{40}][CatB] \quad \text{(Eq. 7)}$$

$$\frac{d[A\beta_{42, deg}]}{dt} = k_{deg, 42}[A\beta_{42}][CatB] \quad \text{(Eq. 8)}$$
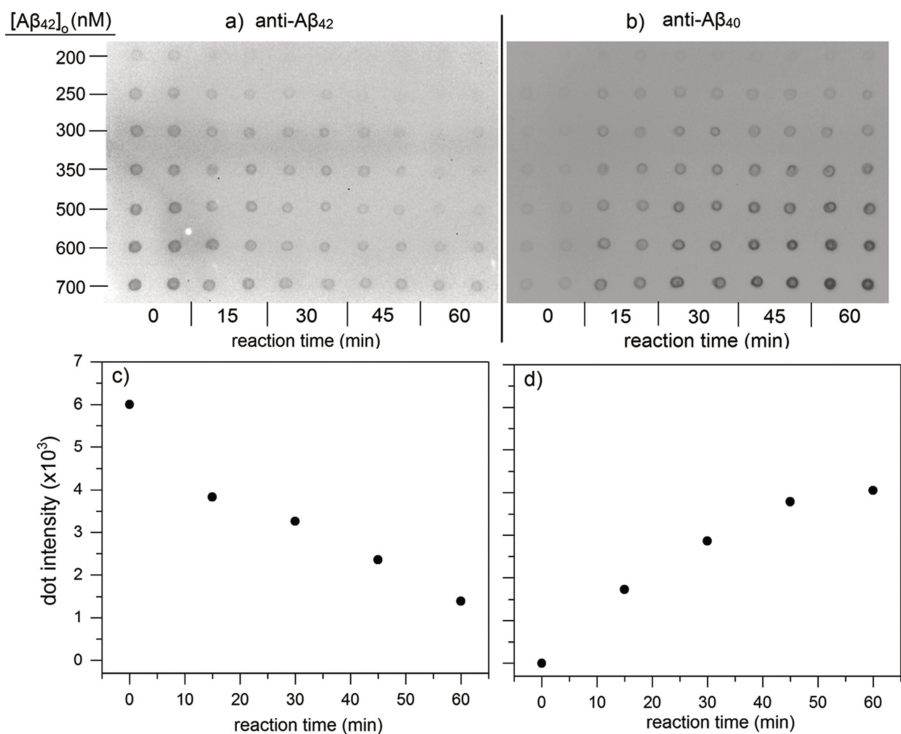
Figure 6. CatB proteolysis of Aβ₄₂. Mixtures of 200 nM CatB and Aβ₄₂ at concentrations shown were incubated at 37 °C, pH 7.4. Samples were dotted onto the membrane at the given time points. Membranes were imaged using an antibody against Aβ₄₂ (*a*) and then stripped and imaged again using an antibody against Aβ₄₀ (*b*). Densitometric scans of the 600 nM sample before and after re-probing are shown in *c* and *d*, respectively. Data are the average of two values.

$$\frac{d[A\beta_{40,\,agg}]}{dt} = k_{1,\,40}[A\beta_{40}] + k_{2,\,40}[A\beta_{40}][A\beta_{40,\,agg}] \quad \text{(Eq. 9)}$$

$$\frac{d[A\beta_{42,\,agg}]}{dt} = k_{1,\,42}[A\beta_{42}] + k_{2,\,42}[A\beta_{42}][A\beta_{42,\,agg}]$$

$$\text{(Eq. 10)}$$

with rate constants determined experimentally and summarized in Table 2. We assumed no cross-aggregation of Aβ₄₀ and Aβ₄₂. The set of equations is initialized by first simultaneous solution of the coupled material balance equations (Equations 3–6) given the initial concentrations of CysC, CatB, and Aβ. Then the differential equations (Equations 7–10) were solved numerically, with iterative solutions of the material balances as intact monomeric Aβ is lost.

We solved the model equations to calculate Aβ aggregation kinetic profiles at several different CysC and CatB concentrations. Specific conditions tested are shown in Table 3. We then measured Aβ aggregation kinetics at these conditions, using ThT fluorescence, and we compared experimental data to model simulations. There were no additional adjustments made to the model.

Model output and data are shown superimposed in Fig. 7. Model simulations accurately captured the experimental data. At 2.5-fold excess Aβ, CysC was able to significantly delay aggregation of Aβ₄₀ but had only a minor impact on Aβ₄₂ aggregation (cases ii and vii). In the absence of CysC, CatB degradation of Aβ was sufficiently fast to completely suppress Aβ aggregation (cases v and ix). When both CatB and CysC were added (at up to 15-fold excess CysC), the lag time for onset of aggregation was delayed, and the steady-state amount of aggregated Aβ was lowered due to degradation (cases iii, iv, and viii).

Table 3

Model validation sample set

Aβ, CysC, and CatB were mixed to the final concentrations given and incubated at 37 °C with 10 μM ThT. Aβ aggregation over time is shown in Fig. 7 and is compared with model predictions.

Sample	[Aβ₄₀]	[Aβ₄₂]	[CysC]	[CatB]
	μM	μM	μM	μM
i	28			
ii	28		12	
iii	28		12	0.8
iv	28		12	1.6
v	28			1.6
vi		10		
vii		10	4	
viii		10	4	1
ix		10		1

Comparison of time constants for degradation versus aggregation

We next sought to develop a simple parameter to predict whether Aβ aggregation or degradation would be the dominant outcome of Aβ–CysC–CatB interactions. We defined a parameter χ, as shown in Equation 11,

$$\chi = \frac{t_{50,\,deg}}{t_{50,\,agg}} \quad \text{(Eq. 11)}$$

where $t_{50,\,deg}$ is the time required for degradation of 50% of Aβ in the absence of any aggregation, and $t_{50,\,agg}$ is the time required for aggregation of 50% of Aβ in the absence of any degradation. χ ⊢ 0 if degradation is the primary outcome, and χ 3 ∞ if aggregation is the primary outcome. Aggregation time is calculated from Equation 12.
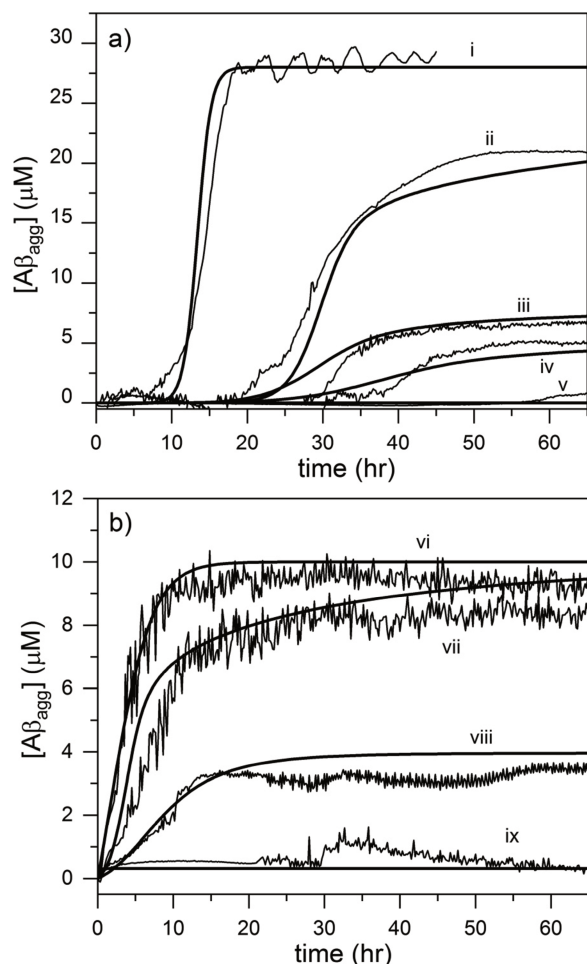
Figure 7. Comparison of model simulations with experimental measurements. *a,* Aβ$_{40}$, and *b,* Aβ$_{42}$ aggregation was monitored by ThT fluorescence at 37 °C, pH 7.4. Experimental data (*thin lines*) are plotted against model prediction (*bold lines*) for the following initial conditions: *trace I,* 28 μM Aβ$_{40}$; *trace ii,* 28 μM Aβ$_{40}$, 12 μM CysC; *trace iii,* 28 μM Aβ$_{40}$, 12 μM CysC, 0.8 μM CatB; *trace iv,* 28 μM Aβ$_{40}$, 12 μM CysC, 1.6 μM CatB; *trace v,* 28 μM Aβ$_{40}$, 1.6 μM CatB; *trace vi,* 10 μM Aβ$_{42}$; *trace vii,* 10 μM Aβ$_{42}$, 4 μM CysC; *trace viii,* 10 μM Aβ$_{42}$, 4 μM CysC, 1 μM CatB; *trace ix,* 10 μM Aβ$_{42}$, 1 μM CatB. All data lines are the average of two independent samples except *trace ii,* in which a single representative sample is shown.

$$t_{50, \text{agg}} = \frac{\ln\left[\dfrac{2k_1 + k_2[A\beta]_0}{k_1}\right]}{k_1 + k_2[A\beta]_0} \quad \text{(Eq. 12)}$$

To a first approximation, degradation time is shown in Equation 13,

$$t_{50, \text{deg}} \approx \frac{\ln(2)(K_I + [\text{CysC}]_0 - [\text{CatB}]_0)}{k_{\text{deg}} K_I [\text{CatB}]_0} \quad \text{(Eq. 13)}$$

(see supplemental text for derivation).

We solved the full-scale numerical model for several different Aβ, CatB, and CysC concentrations and plotted the fraction of aggregated Aβ at long time from the simulations *versus* the calculated χ (Fig. 8*a*). The calculations collapse onto a set of overlapping curves. This plot falls into two clear regimes: aggregation-dominant (χ ≫ 1) and degradation-dominant (χ ≪ 1), with a sharp transition at χ = 1. This behavior was identical for Aβ$_{40}$ and Aβ$_{42}$, meaning that degradation and aggregation
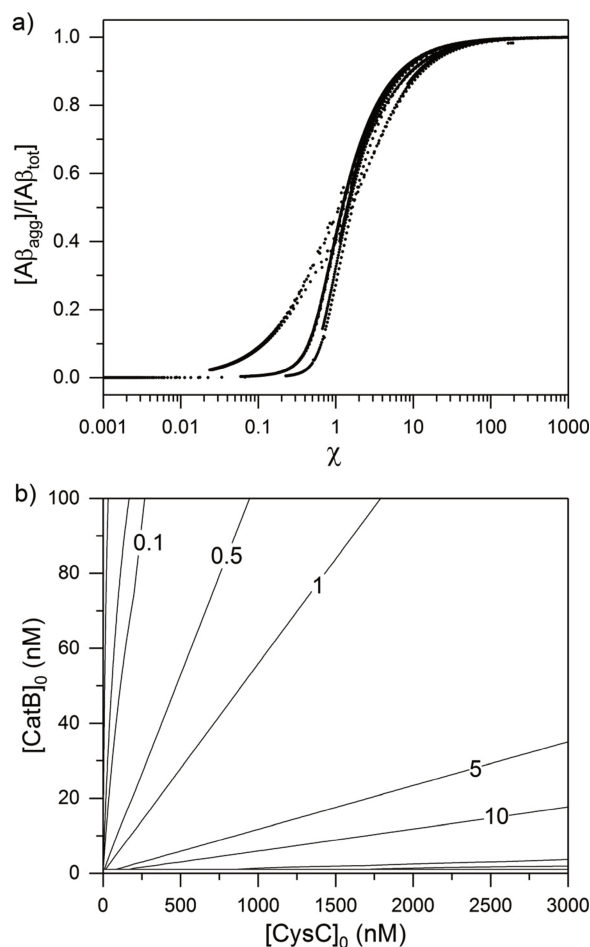
Figure 8. *a,* interaction model was iterated over various initial concentrations of CysC (0–3000 nM), CatB (0–100 nM), and Aβ (20 or 100 nM, for both Aβ$_{40}$ and Aβ$_{42}$). On each iteration, χ was calculated, the model was solved to steady state, and the fraction of aggregated Aβ compared with the total initial Aβ was determined. Each point represents one complete model solution given a unique set of initial conditions. *b,* example set of calculated χ values for initial Aβ$_{40}$ concentration of 10 nM is shown on a contour diagram. Lines of constant χ are shown.

rates used to calculate χ are properly scaled. From this result, we can quantitatively predict whether Aβ will be completely degraded or will end up in toxic aggregated forms, simply from knowledge of initial concentrations of Aβ, CatB, and CysC.

For illustration purposes, we calculated χ at 10 nM Aβ$_{40}$ over a range of CatB and CysC concentrations (Fig. 8*b*). This figures shows, for example, that switching from aggregation (χ ~5) to degradation (χ ~0.5) at constant CatB requires an ~10-fold decrease in CysC.

Discussion

We developed a simple kinetic model to predict the outcome of interactions between CatB, CysC, and Aβ on Aβ aggregation and degradation. Several approximations and assumptions were made in developing the model that deserve brief comment.

ThT fluorescence is commonly used to measure aggregation of Aβ and other amyloidogenic proteins. We found that the maximum ThT intensity was not linear with total fibril mass, in agreement with other work (10, 54, 55). Non-linearity could arise due to differences in ThT-binding modes at high fibril

concentration and accompanying changes in absorbance (56). Additionally, self-quenching effects have been demonstrated at high binding site occupancy (54), which is expected when total fibril mass is small compared with ThT concentration. To account for non-linearity, we fit a polynomial function to a plot of the maximum signal *versus* aggregate mass and then used this fit to correct all other aggregation samples.

Because we used a single experimental output, ThT fluorescence, as a measure of aggregation, we chose to describe the aggregation kinetics using a simple two-parameter model that captures the conversion of Aβ from ThT-negative to ThT-positive aggregates. The autocatalytic model was able to capture the shape and concentration dependence of the experimental data for both $A\beta_{40}$ and $A\beta_{42}$ and to return reasonable values for the two parameters. That said, the fact that the equations fit the data should not be interpreted as indicating that the mechanism is a correct description of the underlying self-association process. In particular, this simple model neglects Aβ oligomer formation, fibril elongation, fibril fragmentation, and other steps in the complex Aβ self-assembly process.

We assumed that CysC binds only the monomeric (unaggregated) form of Aβ. This reduces the complexity of the model, as it eliminates the need to account for different aggregate sizes and to determine the binding affinity as a function of aggregation state. There is some experimental support for this assumption. Mi *et al.* (17) found stable CysC–Aβ complexes in brain homogenates corresponding only to monomer–monomer interactions and only in non-demented control subjects. No such complexes were found in AD patients. The researchers speculated that Aβ–CysC binding was competing with Aβ self-association, with the latter dominating in AD patients. Other protein binders of Aβ are thought to modulate aggregation through more complex mechanisms. For example, transthyretin has been shown to preferentially bind small aggregates of Aβ rather than Aβ monomers (57), resulting in suppression of fibril elongation and lateral association but not initial nucleus formation (58). Although it is possible that CysC can bind Aβ aggregates, it was not necessary to invoke extra binding modes for the model to accurately simulate aggregation data. Our model is consistent with a mechanism whereby CysC sequesters monomeric Aβ, which is slowly released to maintain equilibrium as free Aβ is converted to aggregates or is degraded. It would be of interest to repeat FRET measurements of CysC binding to oligomeric Aβ, if technical difficulties, such as the heterogeneity and instability of the oligomeric Aβ preparation and the effect of aggregation state on donor emission, could be properly managed.

This model assumes that CatB does not degrade Aβ aggregates. Although Aβ fibrils are known to gain extensive resistance to proteolysis (59), CatB degradation of $A\beta_{42}$ fibrils *in vitro* has been reported at pH 7.0 and 37 °C (30). However, we observed no degradation of ThT-positive Aβ aggregates. In Aβ/CysC/CatB co-incubation studies, sample fluorescence reached a plateau and did not decline (Fig. 7, *traces iii, iv,* and *viii*). Some samples maintained a plateau phase for nearly 48 h with no evidence of degradation. Lack of fibril degradation is likely due to a combination of experimental conditions favoring a very small effective concentration of CatB (due to CysC binding) and very low k_{deg} rate constant for fibril proteolysis (due to neutral pH).

Despite these approximations, we were able to accurately predict the aggregation profiles of $A\beta_{40}$ or $A\beta_{42}$ at several different concentrations of CatB and/or CysC (Fig. 7). Moreover, we developed a simplified parameter, χ, which can be quickly used to estimate whether specific concentration regimes will lead to predominantly Aβ aggregation or Aβ degradation. Knowing CysC and CatB levels in an AD animal model, for example, a researcher could find the corresponding value of χ and then determine whether conditions would support Aβ aggregation. CSF biomarker levels in human AD have been determined in multiple studies (23, 24, 36). Typical $A\beta_{40}$ and $A\beta_{42}$ CSF concentrations are 2 and 0.2 nM, respectively (36). CysC concentrations in CSF are reported to be from 200 to 5000 nM in CSF and 100–1000 nM in plasma (23, 24, 36). Total CatB (as determined by ELISA and not residual activity) is ~0.3 nM in CSF and ~6 nM in plasma (36). Using $A\beta_{40}$ = 2 nM, $A\beta_{42}$ = 0.2 nM, CysC = 500 nM, and CatB = 0.5 nM, we obtain χ ~10 for $A\beta_{40}$ and χ ~15,000 for $A\beta_{42}$, showing a strong propensity for Aβ aggregation under typical CSF conditions. If CysC and CatB concentrations were at typical plasma levels (100 and 6 nM, respectively), χ ~0.2 for $A\beta_{40}$, the system moves to the degradation regime. It should be pointed out that the model was developed from experimental data obtained at concentrations higher than physiological for practical reasons. Analyses of χ at typical CSF and plasma conditions require extrapolation of the model to much lower concentrations of Aβ and CatB and should therefore be interpreted cautiously.

The model derived in this study could be expanded to accommodate more complex binding interactions, different cellular environments, and generation of Aβ from APP. For example, CysC is well-known to form domain-swapped dimers (18, 60–63), which lose the ability to inhibit CatB (64). CysC reversibly forms domain-swapped dimers during normal cellular trafficking, but only monomers are secreted (65). The disease-causing L68Q CysC mutation may domain-swap extracellularly, resulting in a pool of predominantly inactive CysC (66–68). If the domain-swapped dimer binds Aβ with the same affinity as monomeric CysC but does not inhibit CatB, CysC and CatB would no longer undermine the neuroprotective effects of one another. Additionally, we have observed oligomeric aggregates of CysC *in vitro*, which are not domain-swapped (18, 20). Nonswapped oligomers remain fully active against CatB, but they inhibit Aβ aggregation much more potently than CysC monomers. It is not clear whether these oligomers exist naturally; if so, oligomer formation could allow CysC to potently control both CatB activity and Aβ aggregation. Engineered CysC mutants also provide a method for testing the model. For example, W106G binds CatB but is a poor inhibitor of its enzymatic activity; we anticipate we would observe rapid degradation of Aβ by CatB if this mutant were used in place of wild-type CysC. We plan to carry out these experiments in the near future.

We considered only the protein interactions at neutral pH typical of extracellular fluids. Most CatB is normally restricted to intracellular compartments. The mildly acidic conditions of the endosomal/lysosomal system could alter considerably the outcome. In acidic cellular compartments, CatB activity is

⫸ASBMB

expected to increase, leading to fast k_{deg} rate constants for both Aβ and CysC substrates (33, 34). Additionally, the assumption of protease-resistant fibrils may be less valid at pH 6 than pH 7.4. However, Aβ aggregation is also accelerated at pH 6 (30). The kinetic model could easily be adapted to predict outcomes at acidic pH once experimental data are collected, allowing determination of k_1, k_2, k_{deg}, K_I, and K_D.

Finally, the model could be adapted to consider Aβ generation. Aβ generation from APP is a complex process resulting from many enzyme interactions (3, 69). It has been suggested that CatB may act as a β-secretase, truncating and priming APP for eventual liberation by a γ-secretase (43–45). This action would be a countervailing effect to CatB's degradation of Aβ.

Experimental procedures

Cystatin C preparation

Recombinant human CysC was produced and purified as described previously (20). Monomeric CysC was fractionated from any dimers or aggregates by membrane filtration and stored at 40 μM in PBSA-E buffer (10 mM phosphate, 150 mM NaCl, 0.02% w/v NaN$_3$, 1 mM EDTA, pH 7.4) at 4 °C. W106G CysC was generated by site-directed mutagenesis (Agilent QuikChange II kit). W106G plasmids were transformed into BL21(DE3) cells (New England Biolabs). W106G was produced and purified as described for WT. Protein concentration was determined by BCA assay (Pierce), using known concentrations of WT as standards. After purification, W106G was stored at 28 μM in PBSA-E at 4 °C.

Aβ aggregation kinetics

Lyophilized Aβ$_{40}$ (Bachem, HCl salt) and Aβ$_{42}$ (Bachem, HCl salt) were reconstituted in denaturing buffer (8 M urea, 100 mM glycine, pH 10) to 2.8 mM, as described previously (9). Small volumes were aliquoted, snap-frozen, and stored at −80 °C. Immediately prior to use, aliquots were thawed and gently diluted to 200 μM in PBS (10 mM phosphate, 150 mM NaCl). ThT powder (Sigma) was dissolved to 100 μM in PBS and filtered through a 0.45-μm syringe filter. Freshly-diluted Aβ and ThT were combined in black 96-well plates to final concentrations of 8, 28, and 46 μM Aβ$_{40}$ or 2.5, 10, and 20 μM Aβ$_{42}$ and 10 μM ThT. The maximum fluorescence intensity is limited by ThT concentration, rather than Aβ (70). For this reason, we chose to hold ThT concentration constant to allow direct comparison of maximum ThT intensity. A clear plastic adhesive strip was used to seal each well and prevent evaporative loss. Fluorescence of ThT was continuously monitored for up to 72 h in a Tecan Infinite M200 plate reader (excitation 440 nm and emission 480 nm), with temperature controlled to 37 °C. Post-aggregation, three reaction mixtures (28 μM Aβ$_{40}$) were removed and centrifuged at 14,000 rpm for 30 min at 4 °C. Residual soluble peptide concentration in the supernatant was determined by BCA assay, using freshly-dissolved Aβ monomers for concentration standards. Fibrillar Aβ concentration (in equivalent monomer molar concentration) was calculated from ThT fluorescence intensity, using maximum ThT fluorescence at 72 h for calibration.

Fluorescent labeling of CysC with Tidefluor 4

Tidefluor 4 succinimidyl ester (TF4 SE) was purchased from AAT Bioquest and dissolved in anhydrous *N,N*-dimethylformamide (DMF, Sigma) to 20 mM. CysC stock was concentrated to 140 μM by ultrafiltration (Amicon Ultra-0.5 ml, 3-kDa MWCO, Millipore) and dialyzed into PBS pH-adjusted to 6.5 with NaH$_2$PO$_4$. TF4 SE solution was added to CysC to final concentrations of 1.4 mM TF4 SE, 130 μM CysC, and 7% v/v DMF. Protein/dye mixture tube was wrapped in aluminum foil and gently shaken at 4 °C for 24 h to conjugate TF4 SE to CysC. Conjugation reaction conditions were chosen to selectively label the N terminus of CysC. Excess dye was removed by gel filtration (Bio-Spin P-6 gel column, Bio-Rad). CysC-TF4 conjugates were eluted in pH 7.4 PBS and stored wrapped in foil at 4 °C. Conjugation efficiency was determined from absorbance at 280 and 590 nm as shown in Equations 14 and 15.

$$[CysC]_{(M)} = \frac{A_{280} - (A_{590} \cdot CF)}{\epsilon_{CysC, 280}} \quad \text{(Eq. 14)}$$

$$\frac{mol_{TF4}}{mol_{CysC}} = \frac{A_{590}}{\epsilon_{TF4, 590} \cdot [CysC]_{(M)}} \quad \text{(Eq. 15)}$$

Molar absorptivities of CysC and TF4 ($\epsilon_{CysC, 280}$ and $\epsilon_{TF4, 590}$) are 11,100 M^{-1} cm^{-1} (46) and 90,000 M^{-1} cm^{-1} (AAT Bioquest), respectively. *CF*, a correction factor for A_{280} of TF4, equals 0.436 (AAT Bioquest). Conjugation efficiency was 72%.

FRET measurements

Hilyte Fluor 488-labeled Aβ$_{40}$ (HF488-Aβ$_{40}$, Anaspec, AS-60491-01) was reconstituted in denaturing buffer (8 M urea, 100 mM glycine, pH 10) to 2.8 mM. Small volumes were aliquoted, snap-frozen, and stored at −80 °C. HF488-Aβ$_{40}$ was thawed and diluted to 10 μM with PBS. Concentration of HF-Aβ$_{40}$ was confirmed by absorbance (ϵ_{497} = 70,000 M^{-1} cm^{-1}, Anaspec) and then adjusted to 800 nM by addition of PBS. TF4-CysC was diluted from stock to 2 μM. TF4-CysC and HF488-Aβ$_{40}$ were mixed to final concentrations of 400 nM HF488-Aβ$_{40}$ and 0–600 nM TF4-CysC. Samples were incubated at 37 °C for 0–60 min and then transferred to a 130-μl cuvette, loaded into the temperature-controlled sample pedestal of a QM-40 fluorometer (PTI, Inc.) and maintained at 37 °C. Fluorescence spectra of all samples were measured using excitation at 488 nm and emission scan of 510–630 nm. Spectra of the same sample taken at various times after mixing showed minor changes up to 10 min and then no difference thereafter (data not shown). Thus, all reported spectra were recorded after at least 10 min of co-incubation. The average of three spectra per sample was recorded. Emission of HF488-Aβ$_{40}$ (FRET donor) at 530 nm was used to determine overall fraction of bound HF488-Aβ$_{40}$ as shown in Equation 16.

$$\frac{[HF488 - A\beta]_{bound}}{[HF488 - A\beta]_{total}} = \frac{I_{530,0} - I_{530}}{I_{530,0} - I_{530,sat}} \quad \text{(Eq. 16)}$$

I_{530} and $I_{530,0}$ are the sample emission at 530 nm in the presence and absence of FRET acceptor (TF4-CysC), respectively. $I_{530,sat}$ is the sample emission under saturating conditions (large excess of TF4-CysC). The fraction of bound HF488-Aβ$_{40}$

was fit to the Hill equation to derive the binding constant, K_D and the cooperativity parameter n as shown in Equation 17.

$$\frac{[\text{HF488} - \text{A}\beta]_{\text{bound}}}{[\text{HF488} - \text{A}\beta]_{\text{total}}} = \frac{[\text{TF4} - \text{CysC}]^n}{K_D + [\text{TF4} - \text{CysC}]^n} \quad \text{(Eq. 17)}$$

Cathepsin B-mediated degradation kinetics

CatB purified from human liver (16.5 μM, Enzo Life Science, BML-SE198-0025) was aliquoted and stored at −80 °C. CatB was activated by mixing equal volumes of CatB stock with activation buffer (10 mM phosphate, 150 mM NaCl, 0.005% v/v Tween 20, 10 mM DTT, pH 7.4) and incubating at room temperature for 15 min. CatB active-site concentration was determined by titration with the irreversible inhibitor, E-64. Stock E-64 (Sigma) was diluted to 1 μM in PBS-T (10 mM phosphate, 150 mM NaCl, 0.005% v/v Tween 20, pH 7.4). Activated CatB (200 nM) was combined with E-64 (0–1000 nM) and incubated at 37 °C for 10 min. Samples were diluted 10-fold at 37 °C PBS-T and then combined in equal volume with 200 μM Z-FR-AMC fluorogenic substrate (R&D Systems). Final concentrations were 10 nM CatB, 0–25 nM E-64, and 100 μM Z-FR-AMC. Fluorescence was monitored over time on a BioTek FL$_X$800 plate reader (excitation 360 nm and emission 460 nm), maintaining samples at 37 °C. Initial rates were plotted against E-64 concentration, and CatB active-site concentration was determined from the x-intercept of the plot. The active-site concentration was found to be ∼95% of the total CatB concentration.

Kinetics of degradation of Aβ_{40}, Aβ_{42}, and CysC (WT and W106G) by CatB were determined by immunoblot assays. Stock Aβ_{40} and Aβ_{42} were thawed and diluted to 10 μM in PBS-T. CatB was activated as described and diluted to 400 nM in PBS-T. CatB and Aβ were combined to final concentrations of 200 nM CatB and 0–5 μM Aβ. In other experiments, activated CatB was mixed with WT or W106G CysC to final concentrations of 200 nM CatB and 0–1000 nM CysC, using either PBS-T (pH 7.4 experiments) or MES-T (25 mM MES, 1 mM EDTA, 1 mM DTT, 0.005% v/v Tween 20, pH 6.0 experiments) as diluent. Mixtures were incubated at 37 °C for up to 2 h. Every 15 min, 2 μl was spotted onto a nitrocellulose membrane and allowed to dry completely. Membranes were washed in TBS-T (20 mM Tris base, 150 mM NaCl, 0.05% v/v Tween 20, pH 8.0) and incubated overnight in blocking buffer (5% w/v nonfat dry milk in TBS-T). Membranes were incubated with antibody against the C terminus of either Aβ_{40} (Abcam, ab76317), Aβ_{42} (Abcam, ab10148), or CysC (Novus, Cyst13) at 2 μg/ml in TBS-T for 1 h at room temperature. The membranes were then washed in TBS-T and incubated with 2 μg/ml goat anti-rabbit (Novus, NBP1-75,325, Aβ blots) or goat anti-mouse (Novus, NB7539, CysC blots) HRP-conjugated secondary antibody in TBS-T for 1 h at room temperature. The membranes were then washed in TBS-T, and antigen was imaged by addition of chemiluminescent substrate (GE Healthcare). Images were taken on a Chemi-Doc XRS+ (Bio-Rad). Blot images were background-subtracted and quantified using ImageJ. Initial degradation rates were plotted against the substrate concentration and data were fit to Equation 18,

$$\frac{d[\text{A}\beta]}{dt} = -k_{\text{deg}}[\text{CatB}]_0[\text{A}\beta] \quad \text{(Eq. 18)}$$

to determine the degradation rate constant k_{deg}.

Model building

All model equations were numerically integrated using ode15s solver package in MATLAB. Equations were input to the solver by a mass matrix to discriminate between material balance and ordinary differential equations. Initial conditions were determined by implicit solution to CysC, Aβ, and CatB material balance equations, given the total amount of each protein. Integration time steps were determined automatically by the solver package. Model equations were solved until steady state was reached.

References

1. Busciglio, J., Gabuzda, D. H., Matsudaira, P., and Yankner, B. A. (1993) Generation of β-amyloid in the secretory pathway in neuronal and non-neuronal cells. *Proc. Natl. Acad. Sci. U.S.A.* **90,** 2092–2096
2. Selkoe, D. J., and Hardy, J. (2016) The amyloid hypothesis of Alzheimer's disease at 25 years. *EMBO Mol. Med.* **8,** 595–608
3. Andrew, R. J., Kellett, K. A., Thinakaran, G., and Hooper, N. M. (2016) A Greek tragedy: The growing complexity of Alzheimer amyloid precursor protein proteolysis. *J. Biol. Chem.* **291,** 19235–19244
4. Mattson, M. P. (1997) Cellular actions of β-amyloid precursor protein and its soluble and fibrillogenic derivatives. *Physiol. Rev.* **77,** 1081–1132
5. Yang, T., Li, S., Xu, H., Walsh, D. M., and Selkoe, D. J. (2017) Large soluble oligomers of amyloid β-protein from Alzheimer brain are far less neuroactive than the smaller oligomers to which they dissociate. *J. Neurosci.* **37,** 152–163
6. Bernacki, J. P., and Murphy, R. M. (2009) Model discrimination and mechanistic interpretation of kinetic data in protein aggregation studies. *Biophys. J.* **96,** 2871–2887
7. Pellarin, R., and Caflisch, A. (2006) Interpreting the aggregation kinetics of amyloid peptides. *J. Mol. Biol.* **360,** 882–892
8. Morris, A. M., Watzky, M. A., and Finke, R. G. (2009) Protein aggregation kinetics, mechanism, and curve-fitting: a review of the literature. *Biochim. Biophys. Acta* **1794,** 375–397
9. Murphy, R. M., and Pallitto, M. M. (2000) Probing the kinetics of β-amyloid self-association. *J. Struct. Biol.* **130,** 109–122
10. Hellstrand, E., Boland, B., Walsh, D. M., and Linse, S. (2010) Amyloid β-protein aggregation produces highly reproducible kinetic data and occurs by a two-phase process. *ACS Chem. Neurosci.* **1,** 13–18
11. Pate, K. M., and Murphy, R. M. (2017) Cerebrospinal fluid proteins as regulators of β-amyloid aggregation and toxicity. *Isr. J. Chem.* **57,** 602–612
12. Levy, E., Sastre, M., Kumar, A., Gallo, G., Piccardo, P., Ghetti, B., and Tagliavini, F. (2001) Codeposition of cystatin C with amyloid-β protein in the brain of Alzheimer disease patients. *J. Neuropathol. Exp. Neurol.* **60,** 94–104
13. Coria, F., Castaño, E. M., and Frangione, B. (1987) Brain amyloid in normal aging and cerebral amyloid angiopathy is antigenically related to Alzheimer's disease β-protein. *Am. J. Pathol.* **129,** 422–428

14. McCarron, M. O., Nicoll, J. A., Stewart, J., Ironside, J. W., Mann, D. M., Love, S., Graham, D. I., and Grubb, A. (2000) Absence of cystatin C mutation in sporadic cerebral amyloid angiopathy-related hemorrhage. Neurology 54, 242–244

15. Maruyama, K., Kametani, F., Ikeda, S., Ishihara, T., and Yanagisawa, N. (1992) Characterization of amyloid fibril protein from a case of cerebral amyloid angiopathy showing immunohistochemical reactivity for both β protein and cystatin C. Neurosci. Lett. 144, 38–42

16. Vinters, H. V., Secor, D. L., Pardridge, W. M., and Gray, F. (1990) Immunohistochemical study of cerebral Alzheimer A4 peptide in cerebral microvessel walls colocalizes with γ trace in patients with leukoencephalopathy. Ann. Neurol. 28, 34–42

17. Mi, W., Jung, S. S., Yu, H., Schmidt, S. D., Nixon, R. A., Mathews, P. M., Tagliavini, F., and Levy, E. (2009) Complexes of amyloid-β and cystatin C in the human central nervous system. J. Alzheimers Dis. 18, 273–280

18. Perlenfein, T. J., Mehlhoff, J. D., and Murphy, R. M. (2017) Insights into the mechanism of cystatin C oligomer and amyloid formation and its interaction with β-amyloid. J. Biol. Chem. 292, 11485–11498

19. Selenica, M. L., Wang, X., Ostergaard-Pedersen, L., Westlind-Danielsson, A., and Grubb, A. (2007) Cystatin C reduces the *in vitro* formation of soluble A-β1–42 oligomers and protofibrils. Scand. J. Clin. Lab. Invest. 67, 179–190

20. Perlenfein, T. J., and Murphy, R. M. (2016) Expression, purification, and characterization of human cystatin C monomers and oligomers. Protein Expr. Purif. 117, 35–43

21. Tizon, B., Ribe, E. M., Mi, W., Troy, C. M., and Levy, E. (2010) Cystatin C protects neuronal cells from amyloid-β-induced toxicity. J. Alzheimers Dis. 19, 885–894

22. Juszczyk, P., Paraschiv, G., Szymanska, A., Kolodziejczyk, A. S., Rodziewicz-Motowidlo, S., Grzonka, Z., and Przybylski, M. (2009) Binding epitopes and interaction structure of the neuroprotective protease inhibitor cystatin C with β-amyloid revealed by proteolytic excision mass spectrometry and molecular docking simulation. J. Med. Chem. 52, 2420–2428

23. Zhong, X. M., Hou, L., Luo, X. N., Shi, H. S., Hu, G. Y., He, H. B., Chen, X. R., Zheng, D., Zhang, Y. F., Tan, Y., Liu, X. J., Mu, N., Chen, J. P., and Ning, Y. P. (2013) Alterations of CSF cystatin C levels and their correlations with CSF Aβ40 and Aβ42 levels in patients with Alzheimer's disease, dementia with Lewy bodies and the atrophic form of general paresis. PLoS ONE 8, e55328

24. Craig-Schapiro, R., Kuhn, M., Xiong, C., Pickering, E. H., Liu, J., Misko, T. P., Perrin, R. J., Bales, K. R., Soares, H., Fagan, A. M., and Holtzman, D. M. (2011) Multiplexed immunoassay panel identifies novel CSF biomarkers for Alzheimer's disease diagnosis and prognosis. PLoS ONE 6, e18850

25. Wang, R., Chen, Z., Fu, Y., Wei, X., Liao, J., and Liu, X. (2017) Plasma cystatin C and high-density lipoprotein are important biomarkers of Alzheimer's disease and vascular dementia: a cross-sectional study. Front. Aging Neurosci. 9, 1–10

26. Björk, I., Pol, E., Raub-Segall, E., Abrahamson, M., Rowan, A. D., and Mort, J. S. (1994) Differential changes in the association and dissociation rate constants for binding of cystatins to target proteinases occurring on N-terminal truncation of the inhibitors indicate that the interaction mechanism varies with different enzymes. Biochem. J. 299, 219–225

27. Nycander, M., Estrada, S., Mort, J. S., Abrahamson, M., and Björk, I. (1998) Two-step mechanism of inhibition of cathepsin B by cystatin C due to displacement of the proteinase occluding loop. FEBS Lett. 422, 61–64

28. Turk, V., Stoka, V., Vasiljeva, O., Renko, M., Sun, T., Turk, B., and Turk, D. (2012) Cysteine cathepsins: from structure, function and regulation to new frontiers. Biochim. Biophys. Acta 1824, 68–88

29. Mackay, E. A., Ehrhard, A., Moniatte, M., Guenet, C., Tardif, C., Tarnus, C., Sorokine, O., Heintzelmann, B., Nay, C., Remy, J. M., Higaki, J., Van Dorsselaer, A., Wagner, J., Danzin, C., and Mamont, P. (1997) A possible role for cathepsins D, E, and B in the processing of β-amyloid precursor protein in Alzheimer's disease. Eur. J. Biochem. 244, 414–425

30. Mueller-Steiner, S., Zhou, Y., Arai, H., Roberson, E. D., Sun, B., Chen, J., Wang, X., Yu, G., Esposito, L., Mucke, L., and Gan, L. (2006) Antiamyloidogenic and neuroprotective functions of cathepsin B: implications for Alzheimer's disease. Neuron 51, 703–714

31. Gan, L., Ye, S., Chu, A., Anton, K., Yi, S., Vincent, V. A., von Schack, D., Chin, D., Murray, J., Lohr, S., Patthy, L., Gonzalez-Zulueta, M., Nikolich, K., and Urfer, R. (2004) Identification of cathepsin B as a mediator of neuronal death induced by Aβ-activated microglial cells using a functional genomics approach. J. Biol. Chem. 279, 5565–5572

32. Yakovlev, A. A., Kvichansky, A. A., Lyzhin, A. A., Khaspekov, L. G., and Gulyaeva, N. V. (2013) Glutamate treatment and preconditioning differently affect cathepsin B release and intracellular proteases in primary cultures of cerebellar granular cells. Neurochem. J. 7, 111–120

33. Linebaugh, B. E., Sameni, M., Day, N. A., Sloane, B. F., and Keppler, D. (1999) Exocytosis of active cathepsin B: Enzyme activity at pH 7.0, inhibition and molecular mass. Eur. J. Biochem. 264, 100–109

34. Werle, B., Jülke, B., Lah, T., Spiess, E., and Ebert, W. (1997) Cathepsin B fraction active at physiological pH of 7.5 is of prognostic significance in squamous cell carcinoma of human lung. Br. J. Cancer 75, 1137–1143

35. Tiribuzi, R., Crispoltoni, L., Porcellati, S., Di Lullo, M., Florenzano, F., Pirro, M., Bagaglia, F., Kawarai, T., Zampolini, M., Orlacchio, A., and Orlacchio, A. (2014) Neurobiology of aging monocytes from patients with sporadic Alzheimer's disease. Neurobiol. Aging 35, 345–356

36. Sundelöf, J., Sundström, J., Hansson, O., Eriksdotter-Jönhagen, M., Giedraitis, V., Larsson, A., Degerman-Gunnarsson, M., Ingelsson, M., Minthon, L., Blennow, K., Kilander, L., Basun, H., and Lannfelt, L. (2010) Higher cathepsin B levels in plasma in Alzheimer's disease compared to healthy controls. J. Alzheimers Dis. 22, 1223–1230

37. Mi, W., Pawlik, M., Sastre, M., Jung, S. S., Radvinsky, D. S., Klein, A. M., Sommer, J., Schmidt, S. D., Nixon, R. A., Mathews, P. M., and Levy, E. (2007) Cystatin C inhibits amyloid-β deposition in Alzheimer's disease mouse models. Nat. Genet. 39, 1440–1442

38. Kaeser, S. A., Herzig, M. C., Coomaraswamy, J., Kilger, E., Selenica, M.-L., Winkler, D. T., Staufenbiel, M., Levy, E., Grubb, A., and Jucker, M. (2007) Cystatin C modulates cerebral β-amyloidosis. Nat. Genet. 39, 1437–1439

39. Sun, B., Zhou, Y., Halabisky, B., Lo, I., Cho, S. H., Mueller-Steiner, S., Devidze, N., Wang, X., Grubb, A., and Gan, L. (2008) Cystatin C-cathepsin B axis regulates amyloid β levels and associated neuronal deficits in an animal model of Alzheimer's disease. Neuron 60, 247–257

40. Wang, C., Sun, B., Zhou, Y., Grubb, A., and Gan, L. (2012) Cathepsin B degrades amyloid-β in mice expressing wild-type human amyloid precursor protein. J. Biol. Chem. 287, 39834–39841

41. Embury, C. M., Dyavarshetty, B., Lu, Y., Wiederin, J. L., Ciborowski, P., Gendelman, H. E., and Kiyota, T. (2017) Cathepsin B improves β-amyloidosis and learning and memory in models of Alzheimer's disease. J. Neuroimmune Pharmacol. 12, 340–352

42. Yang, D. S., Stavrides, P., Mohan, P. S., Kaushik, S., Kumar, A., Ohno, M., Schmidt, S. D., Wesson, D., Bandyopadhyay, U., Jiang, Y., Pawlik, M., Peterhoff, C. M., Yang, A. J., Wilson, D. A., St George-Hyslop, P., et al. (2011) Reversal of autophagy dysfunction in the TgCRND8 mouse model of Alzheimer's disease ameliorates amyloid pathologies and memory deficits. Brain 134, 258–277

43. Hook, V. Y., Kindy, M., and Hook, G. (2008) Inhibitors of cathepsin B improve memory and reduce β-amyloid in transgenic Alzheimer disease mice expressing the wild-type, but not the Swedish mutant, β-secretase site of the amyloid precursor protein. J. Biol. Chem. 283, 7745–7753

44. Hook, G., Hook, V., and Kindy, M. (2011) The cysteine protease inhibitor, E64d, reduces brain amyloid-β and improves memory deficits in Alzheimer's disease animal models by inhibiting cathepsin B, but not BACE1, β-secretase activity. J. Alzheimers Dis. 26, 387–408

45. Wang, X.-F., Liu, D.-X., Liang, Y., Xing, L.-L., Zhao, W.-H., Qin, X.-X., Shang, D.-S., Li, B., Fang, W.-G., Cao, L., Zhao, W.-D., and Chen, Y.-H. (2016) Cystatin C shifts APP processing from amyloid-β production towards non-amyloidgenic pathway in brain endothelial cells. PLoS ONE 11, e0161093

46. Wahlbom, M., Wang, X., Lindström, V., Carlemalm, E., Jaskolski, M., and Grubb, A. (2007) Fibrillogenic oligomers of human cystatin C are formed by propagated domain swapping. J. Biol. Chem. 282, 18318–18326

47. Nagai, A., Ryu, J. K., Terashima, M., Tanigawa, Y., Wakabayashi, K., McLarnon, J. G., Kobayashi, S., Masuda, J., and Kim, S. U. (2005) Neuronal cell death induced by cystatin C *in vivo* and in cultured human CNS neurons is inhibited with cathepsin B. Brain Res. 1066, 120–128

48. Murphy, R. M. (2013) in Tandem Repeats in Genes, Proteins, and Disease: Methods and Protocols (Hatters, D. M. and Hannan, A. J., eds) pp. 201–217, Humana Press Inc., Totowa, NJ

49. Mathews, P. M., and Levy, E. (2016) Cystatin C in aging and in Alzheimer's disease. Ageing Res. Rev. **32,** 38–50

50. Sastre, M., Calero, M., Pawlik, M., Mathews, P. M., Kumar, A., Danilov, V., Schmidt, S. D., Nixon, R. A., Frangione, B., and Levy, E. (2004) Binding of cystatin C to Alzheimer's amyloid β inhibits *in vitro* amyloid fibril formation. Neurobiol. Aging **25,** 1033–1043

51. Polgár, L., and Csoma, C. (1987) Dissociation of ionizing groups in the binding. J. Biol. Chem. **262,** 14448–14453

52. Laurent-Matha, V., Huesgen, P. F., Masson, O., Derocq, D., Prébois, C., Gary-Bobo, M., Lecaille, F., Rebière, B., Meurice, G., Oréar, C., Hollingsworth, R. E., Abrahamson, M., Lalmanach, G., Overall, C. M., and Liaudet-Coopman, E. (2012) Proteolysis of cystatin C by cathepsin D in the breast cancer microenvironment. FASEB J. **26,** 5172–5181

53. Hall, A., Håkansson, K., Mason, R. W., Grubb, A., and Abrahamson, M. (1995) Structural basis for the biological specificity of cystatin C. J. Biol. Chem. **270,** 5115–5121

54. Lindberg, D. J., Wenger, A., Sundin, E., Wesén, E., Westerlund, F., and Esbjörner, E. K. (2017) Binding of thioflavin-T to amyloid fibrils leads to fluorescence self-quenching and fibril compaction. Biochemistry **56,** 2170–2174

55. Bourhim, M., Kruzel, M., Srikrishnan, T., and Nicotera, T. (2007) Linear quantitation of Aβ aggregation using thioflavin T: reduction in fibril formation by colostrinin. J. Neurosci. Methods **160,** 264–268

56. Sulatskaya, A. I., Kuznetsova, I. M., and Turoverov, K. K. (2011) Interaction of thioflavin T with amyloid fibrils: stoichiometry and affinity of dye binding, absorption spectra of bound dye. J. Phys. Chem. B. **115,** 11519–11524

57. Yang, D. T., Joshi, G., Cho, P. Y., Johnson, J. A., and Murphy, R. M. (2013) Transthyretin as both a sensor and a scavenger of β-amyloid oligomers. Biochemistry **52,** 2849–2861

58. Liu, L., and Murphy, R. M. (2006) Kinetics of inhibition of β-amyloid aggregation by transthyretin. Biochemistry **45,** 15702–15709

59. Nordstedt, C., Näslund, J., Tjernberg, L. O., Karlström, A. R., Thyberg, J., and Terenius, L. (1994) The Alzheimer Aβ peptide develops protease resistance in association with its polymerization into fibrils. J. Biol. Chem. **269,** 30773–30776

60. Ekiel, I., and Abrahamson, M. (1996) Folding-related dimerization of human cystatin C. J. Biol. Chem. **271,** 1314–1321

61. Ekiel, I., Abrahamson, M., Fulton, D. B., Lindahl, P., Storer, A. C., Levadoux, W., Lafrance, M., Labelle, S., Pomerleau, Y., Groleau, D., LeSauteur, L., and Gehring, K. (1997) NMR structural studies of human cystatin C dimers and monomers. J. Mol. Biol. **271,** 266–277

62. Janowski, R., Kozak, M., Jankowska, E., Grzonka, Z., Grubb, A., Abrahamson, M., and Jaskolski, M. (2001) Human cystatin C, an amyloidogenic protein, dimerizes through three-dimensional domain swapping. Nat. Struct. Biol. **8,** 316–320

63. Janowski, R., Abrahamson, M., Grubb, A., and Jaskolski, M. (2004) Domain swapping in N-truncated human cystatin C. J. Mol. Biol. **341,** 151–160

64. Hall, A., Ekiel, I., Mason, R. W., Kasprzykowski, F., Grubb, A., and Abrahamson, M. (1998) Structural basis for different inhibitory specificities of human cystatins C and D. Biochemistry **37,** 4071–4079

65. Merz, G. S., Benedikz, E., Schwenk, V., Johansen, T. E., Vogel, L. K., Rushbrook, J. I., and Wisniewski, H. M. (1997) Human cystatin C forms an inactive dimer during intracellular trafficking in transfected CHO cells. J. Cell Physiol. **173,** 423–432

66. Asgeirsson, B., Haebel, S., Thorsteinsson, L., Helgason, E., Gudmundsson, K. O., Gudmundsson, G., and Roepstorff, P. (1998) Hereditary cystatin C amyloid angiopathy: monitoring the presence of the Leu-68 Gln cystatin C variant in cerebrospinal fluids and monocyte cultures by MS. Biochem. J. **329,** 497–503

67. Calero, M., Pawlik, M., Soto, C., Castaño, E. M., Sigurdsson, E. M., Kumar, A., Gallo, G., Frangione, B., and Levy, E. (2001) Distinct properties of wild-type and the amyloidogenic human cystatin C variant of hereditary cerebral hemorrhage with amyloidosis, Icelandic type. J. Neurochem. **77,** 628–637

68. Hyytiä, H., Ristiniemi, N., Airas, L., Pettersson, K., and Hellman, J. (2010) Development of an immunoassay for the detection of cystatin C dimers. J. Immunol. Methods **355,** 14–20

69. Haass, C., Kaether, C., Thinakaran, G., and Sisodia, S. (2012) Trafficking and proteolytic processing of APP. Cold Spring Harb. Perspect. Med. **2,** a006270

70. Xue, C., Lin, T. Y., Chang, D., and Guo, Z. (2017) Thioflavin T as an amyloid dye: fibril quantification, optimal concentration and effect on aggregation. R. Soc. Open Sci. **4,** 160696

ASBMB

A mechanistic model to predict effects of cathepsin B and cystatin C on β-amyloid aggregation and degradation

Tyler J. Perlenfein and Regina M. Murphy

Access the most updated version of this article at doi: 10.1074/jbc.M117.811448

Alerts:
- When this article is cited
- When a correction for this article is posted

Click here to choose from all of JBC's e-mail alerts

Supplemental material:

http://www.jbc.org/content/suppl/2017/10/18/M117.811448.DC1

This article cites 69 references, 18 of which can be accessed free at

http://www.jbc.org/content/292/51/21071.full.html#ref-list-1

Supplemental Data

Inhibition of Aggregation or of Degradation: Cystatin C's Competing Effects on β-Amyloid

Tyler J. Perlenfein, Regina M. Murphy

This section contains the following supplementary data:

- Supplemental Figure S1: Fitting of $A\beta_{40}$ aggregation data to multiple aggregation models to determine best fit

- Supplemental Figure S2: CD spectra of wt and W106G CysC

- Supplemental Figure S3: CatB inhibitory activity of wt and W106G CysC

- Supplemental Figure S4: CatB degradation of CysC by dot blot

- Justification for neglecting CatB bound to $A\beta$ in material balance

- Derivation of $t_{50,agg}$ and $t_{50,deg}$;

Supplemental Figure S1. Aggregation model choice by fit to $A\beta_{40}$ aggregation data. ThT fluorescence data were converted to equivalent aggregated $A\beta_{40}$ concentration by the empirically-determined quadratic equation (see main text). Autocatalytic model (solid line), monomer partitioning model (dashed line), and the Gompertz equation (dotted line) were globally fit to aggregation data including initial $[A\beta_{40}]_0 = 28$ and 46 μM to determine model parameters. Data (thin lines) are shown compared to model fits (thick lines) for (a) $[A\beta_{40}]_0 = 28$ and (b) $[A\beta_{40}]_0 = 46$ μM.
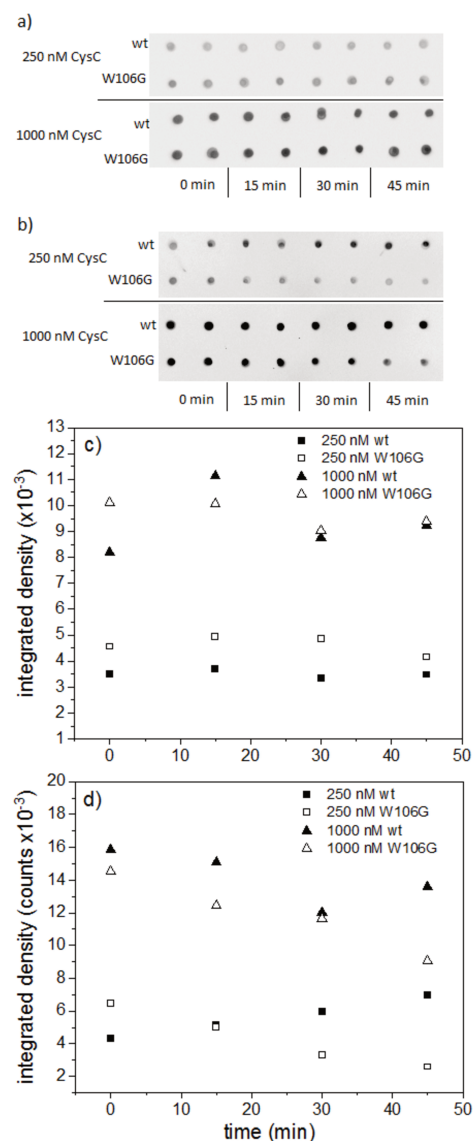
Supplemental Figure S2. CD spectra of wt CysC (solid line) and W106G (dashed line). Protein samples (20 μM in PBSA-E) were dialyzed extensively into 10 mM phosphate, 50 mM NaF, pH 7.4. Measurements of CD spectra were made on an Aviv model 420 and buffer background was subtracted. Data shown is the average of three scans.

Supplemental Figure S3. CatB inhibitory activity of wt CysC (●) and W106G (▲). CysC and activated CatB were mixed to concentrations of 40 nM CatB and 0-100 nM CysC and incubated for 10 minutes at 37°C. Fluorogenic substrate Z-FR-AMC (200 μM) was added to each sample to final concentrations of 20 nM CatB, 100 μM Z-FR-AMC, and 0-50 nM CysC. Sample fluorescence was continuously monitored in a BioTek FL$_x$-800 plate reader for up to ten minutes. Initial rate of fluorescence increase, υ, was determined for each sample and normalized to initial rate without CysC present, υ_0. Each sample shown is the average of two independent samples.

Supplemental Figure S4. CatB degradation of CysC. (a) wt and W106G CysC were incubated with 200 nM CatB for up to one hour at 37°C in pH 7.4 PBS. Samples were taken every 15 minutes and dotted onto a membrane. Membranes were probed for intact CysC using a C-terminal-specific CysC antibody (Cyst13, Novus). (b) Degradation experiments were repeated in pH 6.0 MES buffer. Integrated dot intensities (average of two dots) are shown for pH 7.4 (c) and pH 6.0 (d).

Justification for neglecting CatB bound to Aβ in material balance

Total CatB is distributed between free, bound to CysC, and bound to Aβ. This is expressed by the material balance equation:

$$[CatB]_t = [CatB] + [CatB \cdot CysC] + [CatB \cdot A\beta]$$

We assumed that $[CatB] \gg [CatB \cdot A\beta]$ and that the last term in the material balance equation can be neglected. This assumption is justified from our experimental data as well as data in the literature. For Michaelis-Menten kinetics:

$$\frac{d[P]}{dt} = k_{cat}[ES] = \frac{k_{cat}[E]_{tot}[S]}{K_M + [S]}$$

where

$$K_M = \frac{[E][S]}{[E \cdot S]}$$

and

$$[E]_{tot} = [E] + [E \cdot S] = [E]\left(1 + \frac{[S]}{K_M}\right)$$

If $K_M \gg [S]$, then

$$\frac{d[P]}{dt} \cong \frac{k_{cat}[E]_{tot}[S]}{K_M}$$

and the rate of reaction is linear in substrate concentration. Furthermore,

$$[E]_{tot} \cong [E] \text{ or } [E] \gg [E \cdot S]$$

From Figure 5b, the reaction rate is linear in [Aβ] so we conclude that $K_M \gg 1\ \mu$M and $[CatB] \gg [CatB \cdot A\beta]$.

Some experiments (e.g., Figure 7) were done at higher substrate concentrations (10 and 28 μM), and the assumption was still made that $K_M \gg [S]$ and $[CatB] \gg [CatB \cdot A\beta]$. Literature values for K_M of catB at

pH 7 are consistent with this assumption. For example, Moin et al. (1992) reports K_M of 600-900 μM for catB degradation of dipeptides, while Hasnain et al. (1993) reports K_M of 120-1000 μM for Arg-Phe or Phe-Phe dipeptides. While mass spectrometry analysis of catB degradation of Aβ has been described elsewhere (Mueller-Steiner et al., 2006), we are not aware of any reports of K_M for Aβ.

References:

Moin, K., Day, N.A., Sameni, M., Hasnain, S., Hirama, T., and Sloane, B.F. (1992) Human tumor cathepsin B. Comparison with normal liver cathepsin B. Biochem. J. 285, 427-434.

Hasnain, S., Hirama, T., Huber, C. P., Mason, P., and Mort, J. S. (1993) Characterization of cathepsin B specificity by site-directed mutagenesis. J. Biol. Chem. 268, 235-240.

Mueller-Steiner, S., Zhou, Y., Arai, H., Roberson, E. D., Sun, B., Chen, J., Wang, X., Yu, G., Esposito, L., Mucke, L., and Gan, L. (2006) Antiamyloidogenic and neuroprotective functions of cathepsin B: implications for Alzheimer's disease. Neuron. 51, 703–714

Derivation of $t_{50,deg}$ and $t_{50,agg}$

The autocatalytic model used to describe aggregation kinetics has an analytical solution (Eq. 2). At $t_{50,agg}$, half the Aβ is aggregated and in the absence of any degradation:

$$0.5 = \frac{(k_1 + k_2[A\beta]_0)\exp\left[-(k_1 + k_2[A\beta]_0)t_{50,agg}\right]}{k_2[A\beta]_0\exp\left[-(k_1 + k_2[A\beta]_0)t_{50,agg}\right] + k_1}$$

Algebraic manipulation produces Eq. 12, the half-time for aggregation in the absence of any CatB or CysC:

$$t_{50,agg} = \frac{\ln\left(\frac{2k_1 + k_2[A\beta]_0}{k_1}\right)}{k_1 + k_2[A\beta]_0}$$

Degradation of Aβ by CatB in the absence of any aggregation is modeled as

$$\frac{d[A\beta]}{dt} = -k_{cat}[A\beta][CatB]$$

Making the approximation that [CatB] ~ constant, this equation can be integrated from t = 0 to t = $t_{50,deg}$

$$\ln(0.5) = -k_{cat}[CatB]t_{50,deg}$$

or

$$t_{50,deg} \approx \frac{\ln(2)}{k_{cat}[CatB]}$$

(Eq. S1)

Free (active) CatB concentration depends on CysC concentration (Eq. 3 in main text):

$$[CatB] = [CatB]_0 - \frac{[CysC][CatB]}{K_d}$$

Re-arranging yields

$$[\ ] = [\ ] \cdot \frac{[\ ]}{[\ ] + [\ ]}$$

Combining Eq. S1 and S3 gives:

$$t \approx \frac{\ln(2)\left([\ ] + [\ ]\right)}{[\ ]\,[\ ]}$$

Now we need to solve for [CysC], which depends on CatB and Aβ concentrations (Eq. 4 in main text):

$$[\ ] = [\ ] - \frac{[\ ][\ ]}{[\ ]} - \frac{[\ ][\ ]}{[\ ]}$$

and considering only the Aβ bound to CysC (neglecting the loss of Aβ by degradation or aggregation)

$$[\ ] = [\ ] - \frac{[\ ][\ ]}{[\ ]}$$

Eqs S2, S5 and S6 can be combined to yield a cubic equation:

$$[\ ]^3 + [\ ]^2[\ + \ + [\ ] + [\ ] - [\ ]]$$
$$+ [\ ][\ \ + [\ ] + [\ ] - [\ ] - [\ ]] - [\ ]$$
$$= 0$$

Eq. S7 can be solved for [CysC] using the trigonometric method for cubic equations (or an implicit equation solver), if a more accurate estimate of [CysC] is desired in Eq. S4.

However, to simplify further, we return to Eq. S5. The second term on the rhs is CysC bound to $A\beta$, and the third term on the rhs is CysC bound to CatB. We note that $K_D \gg K_I$, so if $[A\beta] \sim [CatB]$, which is physiologically reasonable, then $\frac{[A\beta][CysC]}{K_D} \ll \frac{[CysC][CatB]}{K_I}$. We also note that the binding affinity for CysC and CatB (K_I) is strong, and that typically $[CysC] > [CatB]$, so the maximum amount of CysC that could be bound to CatB is $[CatB]_0$. With these approximations, Eq S5 simplifies to

$$[CysC] \approx [CysC]_0 - [CatB]_0$$

(Eq. S8)

Plugging Eq S8 into Eq. S4 yields

$$t_{1/2} \approx \frac{\ln(2)\left(K_I + [CysC]_0 - [CatB]_0\right)}{k_{1/2}\,K_I\,[CatB]_0}$$

which is Eq. 13 in the main text.